How Wetting and Adhesion Affect Thermal Conductance of a Range of Hydrophobic to Hydrophilic Aqueous Interfaces

Natalia Shenogina,[1] Rahul Godawat,[2] Pawel Keblinski,[1,†] and Shekhar Garde[2,*]

[1]*Department of Materials Science and Engineering, Rensselaer Polytechnic Institute, Troy, New York 12180, USA*
[2]*Department of Chemical and Biological Engineering, Rensselaer Polytechnic Institute, Troy, New York 12180, USA*

(Received 29 September 2008; published 13 April 2009)

We quantify the strength of interfacial thermal coupling at water-solid interfaces over a broad range of surface chemistries from hydrophobic to hydrophilic using molecular simulations. We show that the Kapitza conductance is proportional to the work of adhesion—a wetting property of that interface—enabling the use of thermal transport measurements as probes of the molecular environment and bonding at an interface. Excellent agreement with experiments on similar systems [Z. B. Ge *et al.*, Phys. Rev. Lett. **96**, 186101 (2006)] highlights the convergence of simulation and experiments on these complex nanoscopic systems.

DOI: 10.1103/PhysRevLett.102.156101 PACS numbers: 68.08.−p, 71.15.Mb

Water structure and dynamics at interfaces are different from those in the bulk and are governed by the nature of the interface (e.g., soft versus rigid) and by interactions with the interface. Statistical mechanical theory predicts dewetting of water from an idealized hydrophobic surface [1] leading to vapor formation at the interface. Attractions with water can pull that interface closer, rewetting it gradually [2–5]. Functionalizing the surface with specific chemistries can alter structure (packing and orientation) as well as dynamics of vicinal water molecules. The behavior of water and the nature of solute-water interface at the molecular level have direct implications on a variety of processes ranging from binding of proteins to surfaces to the broader colloidal and biological self-assembly in interfacial environments [6–8].

At a fundamental level, understanding and characterizing how strongly water hydrates a given interface influences whether biomolecules bind to it or stay away [8], or whether there is stick or slip as water flows past it [9]. From an applied perspective, characterizing the water-interface coupling is important in numerous nanotechnology applications that contain high density of interfaces. To this end, Ge *et al.* [10] have recently measured the resistance for thermal energy transport at hydrophobic and hydrophilic interfaces. As the heat flows across an interface of two materials, the temperature profile at the interface displays a discontinuity [11]. The temperature drop ΔT quantifies the resistance to heat transfer, $R_K = \Delta T/\text{flux}$, called the Kapitza resistance. Its inverse, $G_K = 1/R_K$, the Kapitza conductance [11,12], serves as a measure of the strength of thermal coupling of two phases. Characterizing interfacial coupling via thermal transport studies has several distinct advantages. Thermal energy can be directly imparted to soft or hard objects that may be buried—nanoparticles [13], nanorods, and micelles [14]—and its effects detected, and flow of liquids, as may be required in characterizing stick or slip, is not necessary.

Here we explore and quantify the connection between macroscopic wetting of solid surfaces by water and the interfacial thermal resistance. By using self-assembled monolayers (SAMs) with a broad range of surface chemistries from hydrophobic to hydrophilic, we sample a range of surface wettabilities. We show that their thermal transport properties correlate directly with adhesion energy and with macroscopic wetting characterized by the contact angle. Our study highlights the ability of thermal measurements as probes of interfacial bonding and adhesion.

We employed classical molecular dynamics (MD) simulations of hydration of a set of model surfaces. We used seven different neutral head-group chemistries—($-CF_3$, $-CH_3$, $-OCH_3$, $-CONHCH_3$, $-CN$, $-CONH_2$, and $-OH$)—from most hydrophobic to hydrophililic. The alkane tail was represented using the united atom representation [15]. Head groups were represented at the atomic detail using the AMBER force field [16] except for $-CN$ and $-CF_3$ groups for which optimized potentials for liquid simulations parameters were used [17,18]. Water molecules were represented explicitly using the extended simple point charge model [19]. Electrostatic interactions were calculated using the particle mesh Ewald algorithm [20]. All simulations were performed using GROMACS [21,22]. First, we performed wetting studies to confirm the validity of parameters used. SAM slabs were appropriately annealed leading to an equilibrium crystalline structure with a tilt angle of 28°. Figure 1 shows water droplets on SAM surfaces used to characterize their wetting properties. Consistent with macroscopic expectations based on surface chemistries, we find that the droplets bead up on hydrophobic surfaces and gradually spread on hydrophilic ones. We note that the contact angle for nanodroplets is drop-size dependent. For partially wetting and nonwetting surfaces, its convergence with increasing drop size is understood [23], and is affected by line tension and vapor-liquid surface tension. The contact angles for nanodroplets shown in Fig. 1 agree with experimental data [6]. The agreement

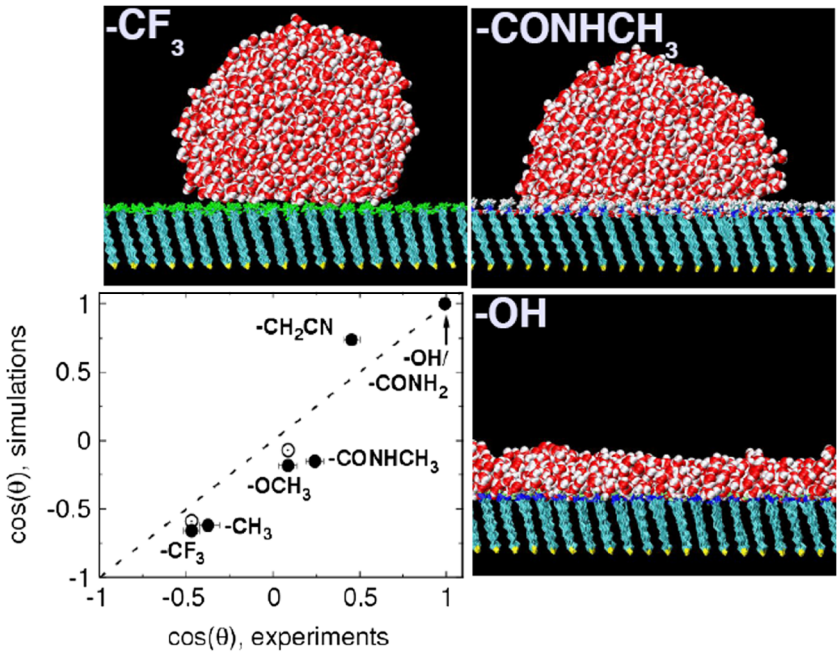

FIG. 1 (color online). Snapshots of water droplets on self-assembled monolayers presenting nonwetting ($-CF_3$), partially wetting ($-CONHCH_3$), and wetting ($-OH$) head groups to water. The plot shows the relationship between $\cos(\theta)$ measured in simulations for droplets of water containing 2176 molecules and in experiments [6] on similar surfaces. Two open circles show limiting macroscopic extrapolations for $-CF_3$ and $-OCH_3$ surfaces obtained from several drop-size-dependent simulations.

improves further for two surfaces, for which limiting values of $\cos(\theta)$ extrapolated using drop-size-dependent simulations are shown. Thus, the force field chosen to represent head groups is reasonable, and correspondingly, their chemical space spans a broad range of hydrophobicity or hydrophilicity.

We used a nonequilibrium setup to study heat flow across water-SAM interfaces [see Fig. 2(a)]. We note that Green-Kubo–based methods have been applied successfully in equilibrium simulations to evaluate thermal resistance of liquid-solid interfaces of a Lennard-Jones (LJ) fluid [24]. Our systems contain two equivalent SAM surfaces, created by attaching surfactant chains (pointing in the positive and negative z direction) to a layer of sulfur atoms, which were position restrained by harmonic springs at locations consistent with those on a Au (111) surface [25,26]. The surfactant chain consists of 10 CH_2 group alkane tail and a head group exposed to water. Our systems included 112 surfactants that create a well-packed crystalline solid $\sim 3.5 \times 3.5$ nm^2 SAM phase. A total of 1500–1700 water molecules were included, leading to the z dimension of the 3D periodic box to be ~ 7 nm.

To prepare the systems for thermal transport studies, we first performed constant pressure and temperature (NPT) runs at 1 atm and 300 K for 500 ps, where SAM and water temperatures were maintained at 300 K using separate Berendsen thermostats [27]. Anisotropic pressure coupling allowed independent variation of the z dimension. The NPT run was followed by a constant temperature and volume (NVT) 500 ps run. Finally, for the remaining 2 ns, the global thermostats were turned off, and a heat source and sink were introduced to induce a steady-state heat flux as described previously [12]. Specifically, atom velocities in a 5 Å thick slab in the center of the water layer were scaled up and those of sulfur atoms of the surfactant slabs were scaled down such that the heat was added to water and removed from surfactants at the same rate, keeping the total system energy constant. A steady state is established over a subnanosecond time scale, with the overall SAM temperature lower than that of water, and heat flowing from water to SAM.

Figures 2(b) and 2(c) show the steady-state temperature profiles of two different SAMs and water along the z direction obtained by time averaging the kinetic energy of atoms residing in 1 Å slices parallel to the SAM surface (in the xy plane) in each phase. A temperature gradient is observed in water and in surfactant chains induced by the heat flow. The temperature dip at the center is due to the artificial resistance associated with linear springs connecting sulfur atoms with hexagonal lattice sites.

Most prominently, there are significant temperature jumps at both the SAM-water interfaces indicating the presence of interfacial thermal resistance also known as the Kapitza resistance [11]. The temperature drop at the hydrophilic ($-OH$) surface is ~ 11 K [Fig. 2(b)], while at the hydrophobic ($-CF_3$) surface with the same heat flux it is ~ 38 K, more than 3 times larger. The inset of Fig. 2(a) also shows density profiles of water near $-OH$ and $-CF_3$ SAM, which we discuss later.

Because heat fluxes used in MD simulations are 1–2 orders of magnitude larger than those typical in experiments, there is a possibility of significant nonlinear effects. To this end, we studied the dependence of temperature drop at the SAM-water interface on the heat flux. Figure 3 shows that the temperature drop is proportional to the heat flux well beyond the values of heat flux employed here, demonstrating that despite large heat fluxes involved, the system is in the linear response regime.

Figure 4 quantifies the relationship between wettability and thermal conductance. Specifically, the conductance is

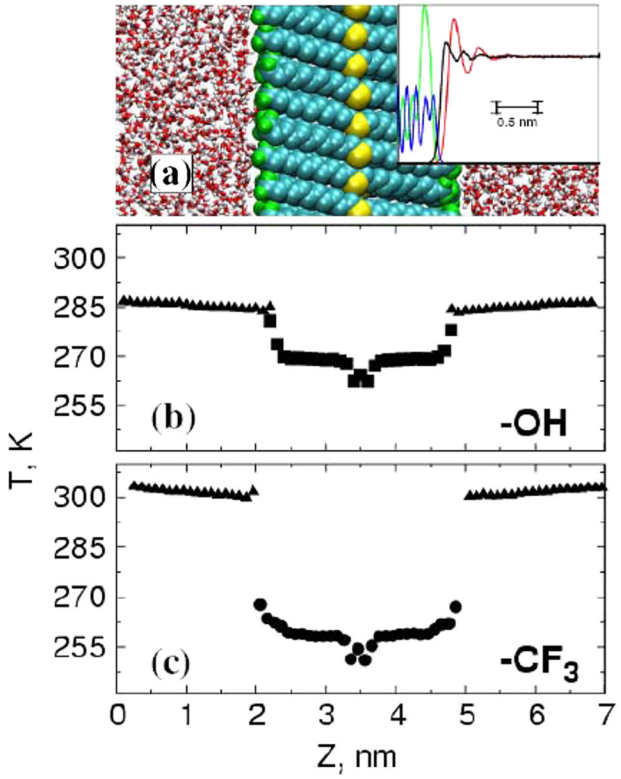

FIG. 2 (color online). (a) A snapshot of the system used in thermal transport simulations (water: red and white; surfactant tails: cyan; head groups: green; sulfur atoms: yellow). Heat source is at the center of the water phase, i.e., at the edge of the simulation box, and the heat is removed from sulfur atoms (yellow) at the center. The inset shows density profiles of water and SAM (for two chemistries) in arbitrary units: SAM densities $-CF_3$ (green) and $-OH$ (blue); vicinal water densities $-CF_3$ (red) and $-OH$ (black). No vapor formation near SAM is evident. (b) Steady-state temperature profile for hydrophilic $-OH$ (SAM)-water interface. (c) Same as in (b) but for hydrophobic $-CF_3$-water interface.

low for nonwetting surfaces and increases with increasing hydrophilicity. A similar behavior was observed in simulations of a LJ fluid interacting with a LJ solid [24,28]. Recognizing that the critical parameter for interfacial heat transfer is the strength of adhesion, in Fig. 4 we plot the thermal conductance as a function of $(1 + \cos\theta)$, where θ is the water droplet contact angle in air. The contact angle is related to interfacial free energies according to Young's equation: $\gamma_{SA} - \gamma_{SW} = \gamma_{AW}\cos\theta$, where subscripts S, W, and A refer to SAM, water, and air, respectively. A simple rearrangement of Young's equation yields

$$W = \gamma_{SA} + \gamma_{AW} - \gamma_{SW} = \gamma_{AW}(1 + \cos\theta). \quad (1)$$

In Eq. (1), W is the work of adhesion, i.e., the energy per unit area needed to detach the water phase from the SAM. Thus, the work of adhesion is proportional to $(1 + \cos\theta)$ with the air-water surface tension being the proportionality coefficient.

Remarkably, Fig. 4 shows that the interfacial conductance is directly proportional to the work of adhesion, or

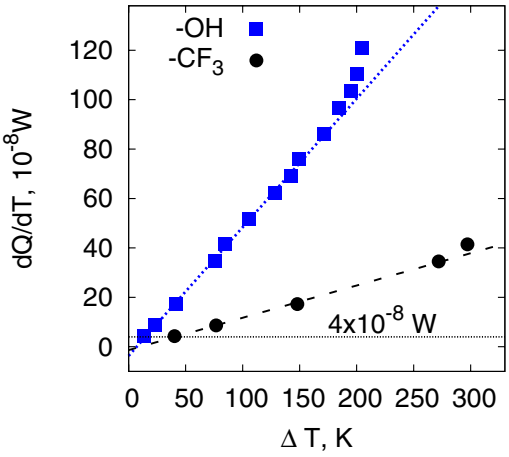

FIG. 3 (color online). Heat flux as a function of the temperature drop at hydrophobic and hydrophilic interfaces. The linear relationship indicates that despite large thermal fluxes involved, the system is within the linear response regime. The horizontal dashed line shows the thermal flux employed in simulations.

equivalently, to $(1 + \cos\theta)$,

$$G_K = B(1 + \cos\theta), \quad (2)$$

with the proportionality coefficient, $B = 85\ \mathrm{MW/m^2\,K}$. The simplicity of Eq. (2) is indeed striking. We note that the two basic models of heat propagation across the interface via phonons—acoustic and diffusive mismatch models [29]—relate the interfacial thermal conductance only to bulk properties of the media forming the interface and have no explicit dependence on the interfacial bonding. On the other hand, an analytical solution of a 1D chain model shows that phonon transmission has rather complicated dependence on the stiffness of the spring connecting the two sides of the chain (representing the two media) [30]. In particular, transmission coefficient of the low frequency

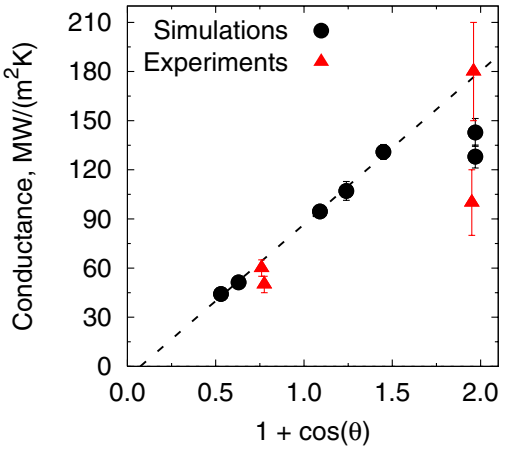

FIG. 4 (color online). Interfacial thermal conductance as a function of $[1 + \cos(\theta)]$. Simulations results (circles) are in good agreement with experimental data [10] (triangles) and show the direct proportionality of interfacial thermal conductance to the work of adhesion.

phonons is essentially independent of the ''interfacial'' spring constant, while higher frequency phonons exhibit lower transmission with decreasing spring constant. For water-SAM systems, our results show that the overall conductance, which can be considered as an integral of the conductance due to all phonons, is simply proportional to the interfacial bonding strength.

Figure 4 also shows four data points from experiments of Ge *et al.* [10]. For hydrophobic SAM surfaces on Au as well as Al metals used in experiments, the agreement between our calculations and experimental data is excellent. The water density in the inset of Fig. 2(a) further shows that water stacks directly against the hydrophobic SAM surface displaying a layered profile. The lack of vapor layer in our simulations, and the excellent agreement with experimental data on thermal transport on similar systems, suggest that there is no vapor layer in experiments as well. Indeed, Fig. 4 would suggest a significantly higher resistance and correspondingly negligible conductance if a vapor layer were to be present (e.g., for $\cos\theta = -1$). For hydrophilic $-$OH surfaces, our data are slightly off the linear correlation with adhesion energy, but, interestingly, exactly in the middle of experimental values for the same systems with Au and Al as metal bases. Overall, the agreement with experimental data is remarkable, and suggests that our simulations mimic key features of those experimental systems.

Through our simulations of thermal energy transport at SAM-water interfaces with a broad range of chemistries, we demonstrated a direct connection between interfacial thermal conductance and wetting properties, hydrophobicity, and adhesion energy of SAM-water interface. In the hydrophobic regime, our results are in remarkably close agreement with experimental data, and along with the structural analysis presented in Fig. 2, suggest that there is no vapor layer present at such interfaces. Although water is expected to form a soft vapor-liquid–like interface near idealized hard hydrophobic surfaces [1], addition of weak attractive interactions pulls that interface closer, leading to rewetting [2–5]. This observation is also consistent with the structure of water at other hydrophobic interfaces studied by experiments [31] and simulations [32].

More generally, we demonstrated that thermal transport measurements can be used to probe interfacial environments and to quantify interfacial bonding strength. This provides a unique opportunity to characterize a variety of interfaces, such as those between nanoparticles embedded in liquids or materials using laser-based techniques, which are difficult to access with direct structural characterization tools. Quantifying the interfacial density fluctuations, which constitute an alternate characterization of the vicinal molecular environment [33,34], will provide additional insights into connections between thermal coupling and molecular structure and dynamics.

We acknowledge financial support of the NSF Nanoscale Science and Engineering Center Grant No. DMR-011779. P. K. also acknowledges support from the AFOSR/MURI program under Grant No. FA9550-08-1-0407.

*gardes@rpi.edu
†keblip@rpi.edu

[1] F. H. Stillinger, J. Solution Chem. **2**, 141 (1973).
[2] D. Chandler, Nature (London) **437**, 640 (2005).
[3] D. M. Huang and D. Chandler, J. Phys. Chem. B **106**, 2047 (2002).
[4] G. Hummer and S. Garde, Phys. Rev. Lett. **80**, 4193 (1998).
[5] G. Goel *et al.*, J. Phys. Chem. B **112**, 13193 (2008).
[6] G. B. Sigal, M. Mrksich, and G. M. Whitesides, J. Am. Chem. Soc. **120**, 3464 (1998).
[7] R. S. Kane, P. Deschatelets, and G. M. Whitesides, Langmuir **19**, 2388 (2003).
[8] A. Sethuraman *et al.*, Langmuir **20**, 7779 (2004).
[9] J. Koplik and J. R. Banavar, Phys. Rev. Lett. **96**, 044505 (2006).
[10] Z. B. Ge, D. G. Cahill, and P. V. Braun, Phys. Rev. Lett. **96**, 186101 (2006).
[11] D. G. Cahill *et al.*, J. Appl. Phys. **93**, 793 (2003).
[12] H. A. Patel, S. Garde, and P. Keblinski, Nano Lett. **5**, 2225 (2005).
[13] S. A. Putnam *et al.*, J. Appl. Phys. **99**, 084308 (2006).
[14] A. J. Schmidt *et al.*, J. Phys. Chem. C **112**, 13320 (2008).
[15] M. Mondello *et al.*, J. Chem. Phys. **109**, 798 (1998).
[16] W. D. Cornell *et al.*, J. Am. Chem. Soc. **117**, 5179 (1995).
[17] M. L. P. Price, D. Ostrovsky, and W. L. Jorgensen, J. Comput. Chem. **22**, 1340 (2001).
[18] E. K. Watkins and W. L. Jorgensen, J. Phys. Chem. A **105**, 4118 (2001).
[19] H. J. C. Berendsen, J. R. Grigera, and T. P. Straatsma, J. Phys. Chem. **91**, 6269 (1987).
[20] U. Essmann *et al.*, J. Chem. Phys. **103**, 8577 (1995).
[21] E. Lindahl, B. Hess, and D. van der Spoel, J. Mol. Model. **7**, 306 (2001).
[22] H. J. C. Berendsen, D. Vanderspoel, and R. Vandrunen, Comput. Phys. Commun. **91**, 43 (1995).
[23] T. Werder *et al.*, J. Phys. Chem. B **107**, 1345 (2003).
[24] J. L. Barrat and F. Chiaruttini, Mol. Phys. **101**, 1605 (2003).
[25] P. E. Laibinis *et al.*, J. Am. Chem. Soc. **113**, 7152 (1991).
[26] J. C. Love *et al.*, Chem. Rev. **105**, 1103 (2005).
[27] H. J. C. Berendsen *et al.*, J. Chem. Phys. **81**, 3684 (1984).
[28] L. Xue *et al.*, J. Chem. Phys. **118**, 337 (2003).
[29] E. T. Swartz and R. O. Pohl, Rev. Mod. Phys. **61**, 605 (1989).
[30] C. Caroli *et al.*, J. Phys. C **4**, 916 (1971).
[31] K. Kashimoto *et al.*, Phys. Rev. Lett. **101**, 076102 (2008).
[32] H. A. Patel, E. B. Nauman, and S. Garde, J. Chem. Phys. **119**, 9199 (2003).
[33] J. Mittal and G. Hummer, Proc. Natl. Acad. Sci. U.S.A. **105**, 20 130 (2008).
[34] A. P. Willard and D. Chandler, Faraday Discuss. **141**, 209 (2009).